Experimental Thermal and Fluid Science 88 (2017) 513–518

Contents lists available at ScienceDirect

Experimental Thermal and Fluid Science

journal homepage: www.elsevier.com/locate/etfs

Tidal bore progressing on a small slope

Ying Li [a], Dong-Zi Pan [b,*], Hubert Chanson [c], Cun-Hong Pan [b]

[a] Zhejiang University of Water Resources and Electric Power, 583 Xuelin Street, Hangzhou 310018, China
[b] Zhejiang Institute of Hydraulics and Estuary, 50 East Fengqi Road, Hangzhou 310020, China
[c] The University of Queensland, School of Civil Engineering, Brisbane, QLD 4072, Australia

ARTICLE INFO

Article history:
Received 24 November 2016
Received in revised form 28 May 2017
Accepted 10 July 2017
Available online 11 July 2017

Keywords:
Open channel
Tidal bore
Hydraulic jump
Froude number
Bed slope

ABSTRACT

In a natural estuary, a tidal bore may progress on a small sloping bed from the downstream to the upstream. In this study, a simple analytical solution for tidal bore formed in a small slope channel was developed using the finite control volume analysis. New unsteady experiments were conducted to verify the theoretical model. The model predictions generally agree with the observations. A general relation is obtained for the conjugate depth ratio as a function of the Froude number and the channel slope from the experimental data. The results indicate that the conjugate depth ratio increases with an increasing Froude number as well as with a decrease in channel slope. On a negative slope, the Froude number increases as the bore propagates along the channel, and decreases for a positive slope. The theoretically based model is accurate and simple to estimate the celerity of the tidal bore progressing along a small slope channel.

1. Introduction

A tidal bore is a special geophysical phenomenon in which the leading edge of the flood tide forms an undular or breaking bore that travels up a river or narrow bay against the direction of the initial flow current [1]. An undular bore is a positive surge characterised by a train of secondary waves following the surge front [2]. A breaking bore is a wall of turbulent water rushing upstream along the river with its foaming front and rumble noise [3]. A tidal bore is a moving hydraulic jump. This problem was studied by scientific researchers and hydraulic engineers for a couple of centuries. Using the shallow-water equations, Barré de Saint-Venant [4] first predicted the theoretical development of a tidal bore. Other theoretical analysis and literature reviews comprise [5–7]. Although most studies considered horizontal channels, the bed of natural estuaries with tidal bore generally presents some slope. In the Qiantang River, China, the bore results from the funnel-shaped character of the Hangzhou Bay and a sand bar that occupies the mouth [8–10]. The rising sand bar with an average riverbed slope of 0.0002 decreases the water depth, and the funnel-shaped bay concentrates the water energy as well, resulting in the strong Qiantang River tidal bore.

While hydraulic jumps on sloping channels have been studied [11–13], there is limited research about the tidal bore progressing on a slope [14]. Combining a theoretical derivation and new physical data, the tidal bore progressing on a small slope with different slope angle θ ($-0.004 < \theta < 0.004$) is investigated here.

2. Theoretical models for a small slope channel

Let us consider a tidal bore progressing upstream on a prismatic channel with small slope θ depicted in Fig. 1. Take a fixed and deforming control volume with length L and width B, between an upstream section 1 and the end of the channel section 2. In Fig. 1, d, V and P are the flow depth, velocity and water pressure, respectively; f is the boundary shear force; G is the gravity force; C, t and L are respectively the celerity, progressing time and distance of the tidal bore; d_j is the conjugate water depth, that is the flow depth immediately behind the bore front; the subscripts 1 and 2 refer to the flow conditions at sections 1 and 2 (Fig. 1a).

For a small slope θ ($-0.004 < \theta < 0.004$), the control volume $\bar{V}$ is (Fig. 1a)

$$\bar{V} = B(\Omega_1 + \Omega_2) \tag{1}$$

where $\Omega_1 = d_1(L - Ct) - 0.5m(L - Ct)^2$, $\Omega_2 = d_2Ct + 0.5mC^2t^2$, $m = \tan\theta + \tan\varphi$. φ is the friction slope [2]

$$\tan\varphi = \frac{4\tau_0}{\rho g D} \tag{2}$$

* Corresponding author.
E-mail address: pandz@zjwater.gov.cn (D.-Z. Pan).

http://dx.doi.org/10.1016/j.expthermflusci.2017.07.004
0894-1777/

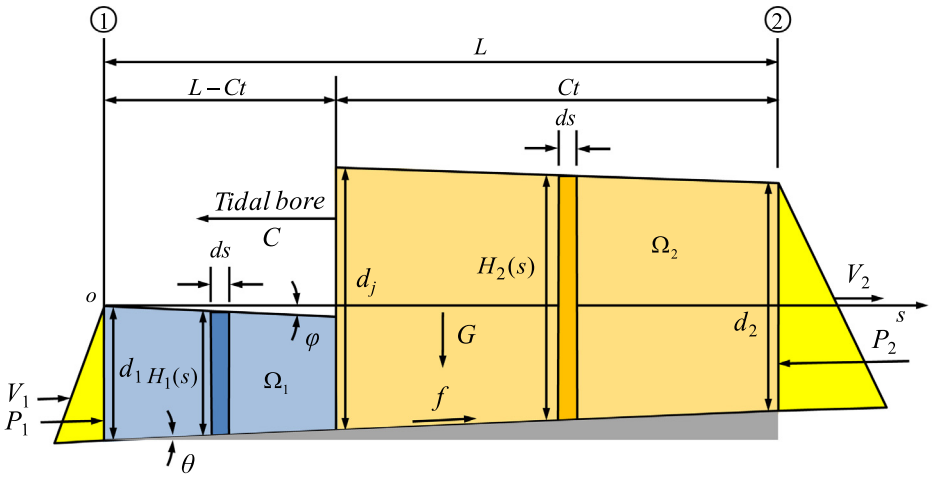

(a) Physical variables and geometrical description.

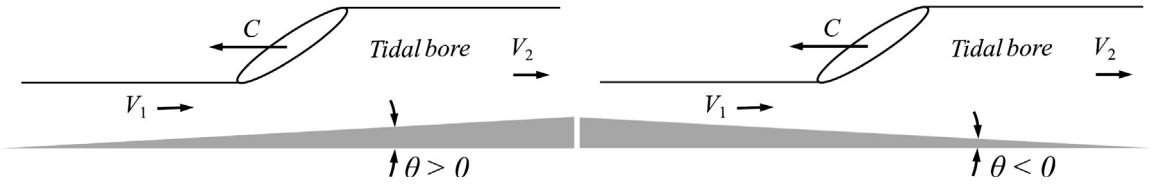

(b) Downward propagation. (c) Upward propagation.

Fig. 1. Sketch of tidal bore progressing upstream along a prismatic channel. (a) Physical variables and geometrical description. (b) Downward propagation. (c) Upward propagation.

where τ_0 is the boundary shear stress, $\tau_0 = \lambda\rho V^2/8$, λ is the Darcy-Weisbach friction factor, and D is the hydraulic diameter.

2.1. Conservation of mass

For the control volume (CV), the equation of conservation of mass may be expressed as

$$\frac{d}{dt}\int_{CV}\rho d\bar{V} = -\int_{Ain}\rho(\vec{V}\cdot\vec{n})dA - \int_{Aout}\rho(\vec{V}\cdot\vec{n})dA \tag{3}$$

where ρ is the density of water; $\vec{V}$ is the velocity vector; $\vec{n}$ is the normal vector; and $\rho(\vec{V}\cdot\vec{n})dA$ is the mass flow rate through the differential area dA. The sign of the dot product $\vec{V}\cdot\vec{n}$ is "+" for flow out of the control volume and "−" for flow into the control volume.

Assuming ρ to be a constant and considering the velocity distribution at the sections 1 and 2 are uniform, then $\int_{Ain}\rho(\vec{V}\cdot\vec{n})dA = -B\rho V_1 d_1$, and $\int_{Aout}\rho(\vec{V}\cdot\vec{n})dA = -B\rho V_2 d_2$.

From Eq. (1), it yields

$$\frac{d}{dt}\int_{CV}\rho d\bar{V} = \rho BC(d_2 - d_1 + Lm) \tag{4}$$

Substituting Eq. (4) to Eq. (3), it gives

$$d_2(V_2 + C) = d_1(V_1 + C) - CLm \tag{5}$$

2.2. The linear momentum equation

From Newton's second law, the linear momentum equation may be written in an integral form as

$$\frac{d}{dt}\int_{CV}\rho\vec{V}\,d\bar{V} = \sum\vec{F}_{ex} - \int_{Ain}\rho(\vec{V}\cdot\vec{n})\vec{V}\,dA - \int_{Aout}\rho(\vec{V}\cdot\vec{n})\vec{V}\,dA \tag{6}$$

where $\sum\vec{F}_{ex}$ is the total external forces acting on the control volume; $\int_{Ain}\rho(\vec{V}\cdot\vec{n})\vec{V}\,dA = -\rho BV_1V_1d_1$, and $\int_{Aout}\rho(\vec{V}\cdot\vec{n})\vec{V}\,dA = -\rho BV_2V_2d_2$.

From Eq. (1), it yields

$$\frac{d}{dt}\int_{CV}\rho\vec{V}\,d\bar{V} = \rho B\frac{d}{dt}\int_{\Omega_1}\vec{V}\,dA + \rho B\frac{d}{dt}\int_{\Omega_2}\vec{V}\,dA \tag{7}$$

The conservation of mass implies that the discharge any section in Ω_1 and Ω_2 is equal, i.e., $q_1(s) = V_1d_1$, $q_2(s) = V_2d_2$, where $q_1(s)$ and $q_2(s)$ are the discharge per meter width at section 1 and 2, respectively. Based upon geometric considerations (Fig. 1):

$$\int_{\Omega_1}\vec{V}\,dA = \int_0^{L-Ct}V(s)H_1(s)ds = \int_0^{L-Ct}q_1(s)ds = V_1d_1(L - Ct) \tag{8}$$

$$\int_{\Omega_2}\vec{V}\,dA = \int_{L-Ct}^{L}V(s)H_2(s)ds = \int_{L-Ct}^{L}q_2(s)ds = V_2d_2(L - Ct) \tag{9}$$

Substituting Eqs. (8) and (9) into Eq. (7), it yields

$$\frac{d}{dt}\int_{CV}\rho\vec{V}\,d\bar{V} = \rho BC(V_2d_2 - V_1d_1) \tag{10}$$

The total external force acting on the control volume shown in Fig. 1 along the surface of the slope is

$$\sum\vec{F}_{ex} = P_1 + P_2 + f + G\sin\theta \tag{11}$$

where $P_1 = 0.5\rho g B d_1^2 \cos\theta$, $P_2 = -0.5\rho g B d_2^2 \cos\theta$, $f = \tau_0 P_w L$, and $G = -k\rho g \bar{V}$; k is the area correction coefficient for the straight line assumption of tidal bore profile, P_w is the wetted perimeter. When the front of tidal bore reaches section 1 in Fig. 1a, $\bar{V} = BLd_2 + 0.5mBL^2$, $f = 0.125\rho\lambda V_2^2(2d_2 + B)L$.

Substituting Eqs. (10) and (11) into Eq. (6), and combining with Eq. (5), the equation of momentum conservation becomes

$$d_1(V_1 + C)(V_2 - V_1) - mCLV_2 = 0.5g(d_1^2 - d_2^2)\cos\theta - gkL \times \sin\theta(d_2 + 0.5Lm) + 0.125\lambda V_2^2(2d_2/B + 1)L \quad (12)$$

If $\theta = 0$ in Eq. (12) and neglecting the flow resistance, then $f = 0$ and $m = 0$, the above equation yields the classical Bélanger equation [2,15,16]

$$\frac{d_2}{d_1} = \frac{1}{2}\left(\sqrt{1 + 8Fr^2} - 1\right) \quad (13)$$

where $Fr = (V_1 + C)/\sqrt{gd_1}$ for a rectangular channel.

3. Laboratory model

New laboratory experiments were performed in a tilting flume located in the Seddon Hydraulics Laboratory at the University of Queensland. The channel was 0.5 m wide and 12 m long. The flume was made of smooth PVC bed and glass walls. The waters were supplied by a constant head tank, feeding an upstream water tank leading to the glass-sidewall test section through a series of flow straighteners followed by a smooth three-dimensional convergent. A fast closing Tainter gate was located next to the downstream end of the channel at $x = 11.15$ m.

The tidal bore was generated by the fast gate closure and the bore propagated upstream against the direction of the initial flow current. The gate closure time was less than 0.2 s. The gate opening h after closure and the channel slope angle θ were adjustable. The channel slope angle was checked carefully against the longitudinal changes in water depth in still water conditions, as shown in Fig. 2 where d is the water depth; x is the longitudinal distance from the upstream end of channel; θ is the angle of the channel with the horizontal, $\theta > 0$ for a downward sloping flume and $\theta < 0$ for an upward sloping channel.

The water discharge was measured with an orifice meter installed on the supply line and previously calibrated in-situ with a large V-notch weir. The water depths were measured using rail mounted pointer gauges in steady flows and Microsonic™ Mic +25/IU/TC acoustic displacement meters in steady flows and unsteady flows. The displacement meters were calibrated with steady flows on-site against pointer gauge measurements for a range of water depths.

4. Experimental results

Fig. 3 shows the variation of the conjugate depth ratio d_j/d_1 as function of the Froude number Fr for tidal bore progressing on a small slope. For positive slope angles (Fig. 3a), the conjugate depth ratio d_j/d_1 increases with the decrease of the slope $\theta(\theta > 0)$ at a particular Froude number. For negative slopes (Fig. 3b), it also increases with the decrease of the slope $\theta(\theta < 0)$ at a particular Froude number.

As seen in Fig. 3, the lowest d_j/d_1 values are linked to the maximum positive slope ($\tan\theta = 0.0036$) and the highest d_j/d_1 values are associated with the minimum negative slope ($\tan\theta = -0.0036$). This results from the direction of the gravity force component in the flow direction and the initial flow

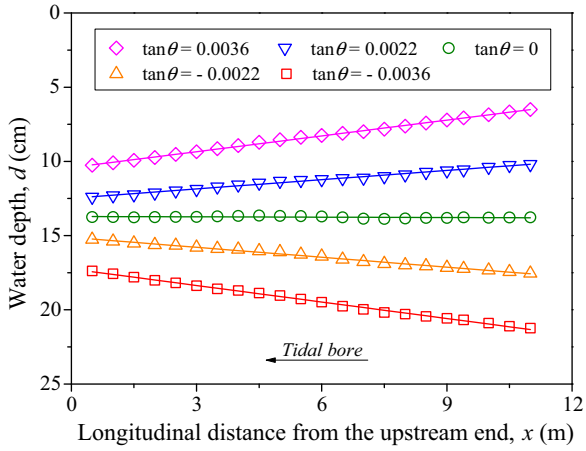

(a) Measured bed slopes.

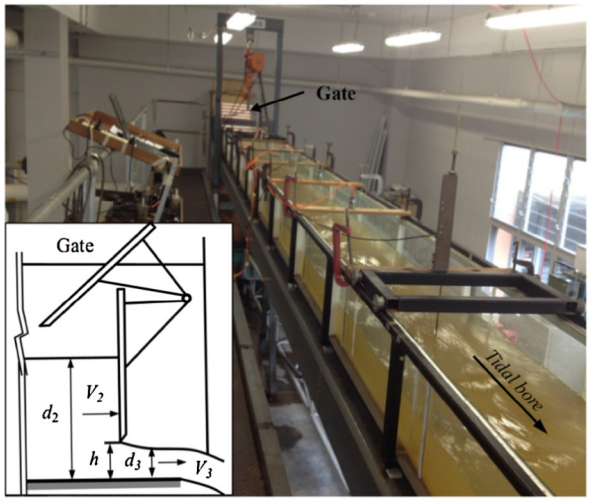

(b) Photograph of the flume (Inset: details of Tainter gate, d_3 and V_3 are the flow depth and velocity beneath the gate).

Fig. 2. The sloping channel. (a) Measured bed slopes. (b) Photograph of the flume (Inset: details of Tainter gate, d_3 and V_3 are the flow depth and velocity beneath the gate).

conditions. In case of the negative slope, the weight component accelerates the initial flow, while, in case of the positive slope, it increases the resistance to the initial flow.

The experimental data were best correlated by a simple regression

$$\frac{d_j}{d_1} = \frac{1}{2}\left(\sqrt{1 + AFr^2} - B\right) \quad (14)$$

where $A = 6.92 + \frac{0.0017}{\tan\theta + 0.0045}$; $B = 11.1\tan\theta + 0.5$. Eq. (14) is compared to the experimental observations in Fig. 3. Eq. (14), similar to the classical Bélanger equation, gives a simple relationship for the determination of the conjugate depth ratio using the initial Froude number and the bed slope.

5. Discussion

When the downstream gate is fully-closed after closure (Fig. 2b), the gate opening h after closure is zero, and $V_2 = 0$. When $h > 0$, the discharge beneath the gate may be estimated using a quasi-steady flow approximation based upon continuity and Ber-

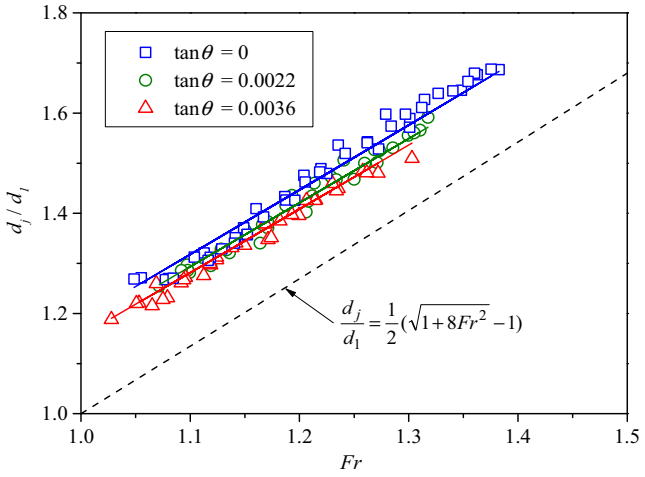

(a) Positive slope angle.

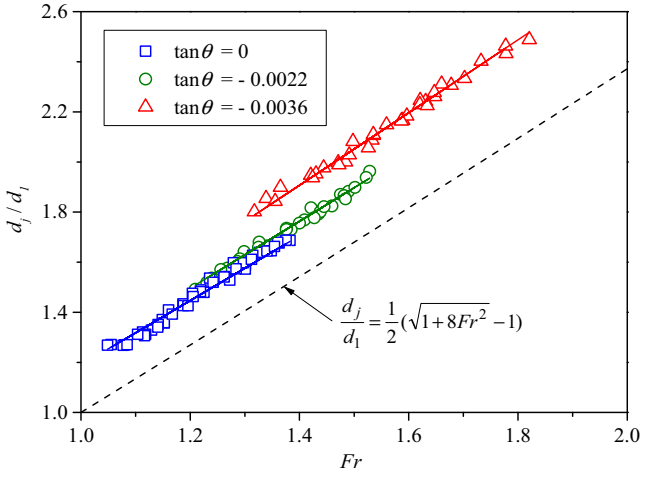

(b) Negative slope angle.

Fig. 3. Variation of the conjugate depth ratio d_j/d_1 as a function of the Froude number Fr for tidal bore progressing on a small slope. Comparison with Eq. (14) (solid lines) and the Bélanger equation (Eq. (13)) (dashed line). (a) Positive slope angle. (b) Negative slope angle.

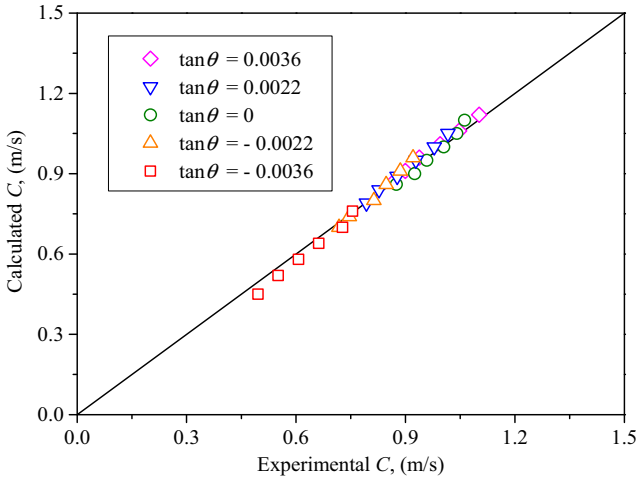

(a) Bore celerity.

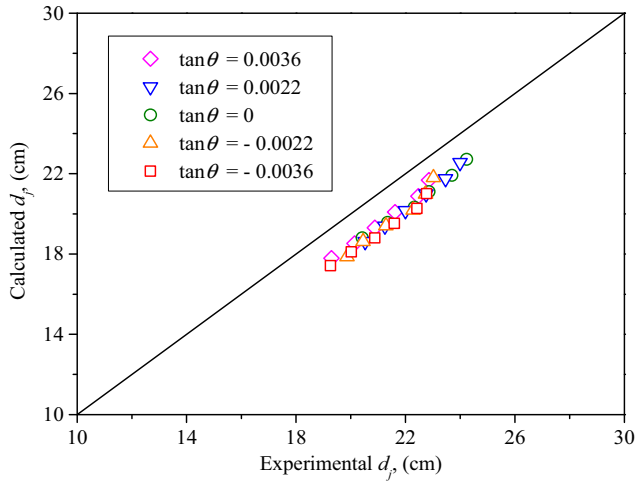

(b) Conjugate water depth.

Fig. 4. Comparison of experimental results with theoretical calculations. (a) Bore celerity. (b) Conjugate water depth.

noulli considerations [17]. That is, the continuity equation and Bernoulli principle may be assumed to satisfy

$$V_2 d_2 B = V_3 d_3 B \tag{15}$$

$$d_2 + z_0 + \frac{V_2^2}{2g} = d_3 + z_0 + \frac{V_3^2}{2g} \tag{16}$$

where z_0 is the invert elevation.

Assuming

$$d_3 = C_c h \tag{17}$$

where C_c is the contraction coefficient (Table 1) that may be derived from irrotational flow theory for the Tainter gate geometry [18,19].

From Eqs. (15), (16) and (17), it yields

Table 1
Contraction coefficient C_c versus the gate opening h after [18].

h (cm)	0	1	2	3	4
C_c	0.611	0.611	0.610	0.608	0.606

$$V_2 = C_c h\sqrt{\frac{2g}{d_2 + C_c h}} \tag{18}$$

For each experiment and location along the channel, V_1 and d_1 are known variables; from Eqs. (5), (12) and (18), C and d_2 can be solved. Based upon geometric relationships in Fig. 1, the conjugate water depth d_j is

$$d_j = d_2 + mL \tag{19}$$

Finally, the theoretical calculations for the bore celerity C and conjugate water depth d_j of the tidal bore at the longitudinal distance from gate x = 3.65 m are compared to experimental data in Fig. 4 for different channel slopes. Overall there is a good agreement between computations and measurements in terms of the celerity of tidal bore. The absolute average errors were 0.01, 0.02, 0.01, 0.02 and 0.03 m/s for the channel slopes of 0.0036, 0.0022, 0, −0.0022 and −0.0036, respectively. Note that the calculated conjugate water depth presents a fair agreement with the experimental data, although the calculated results do not compare as well as those of bore celerity. All the conjugate depth observations were a

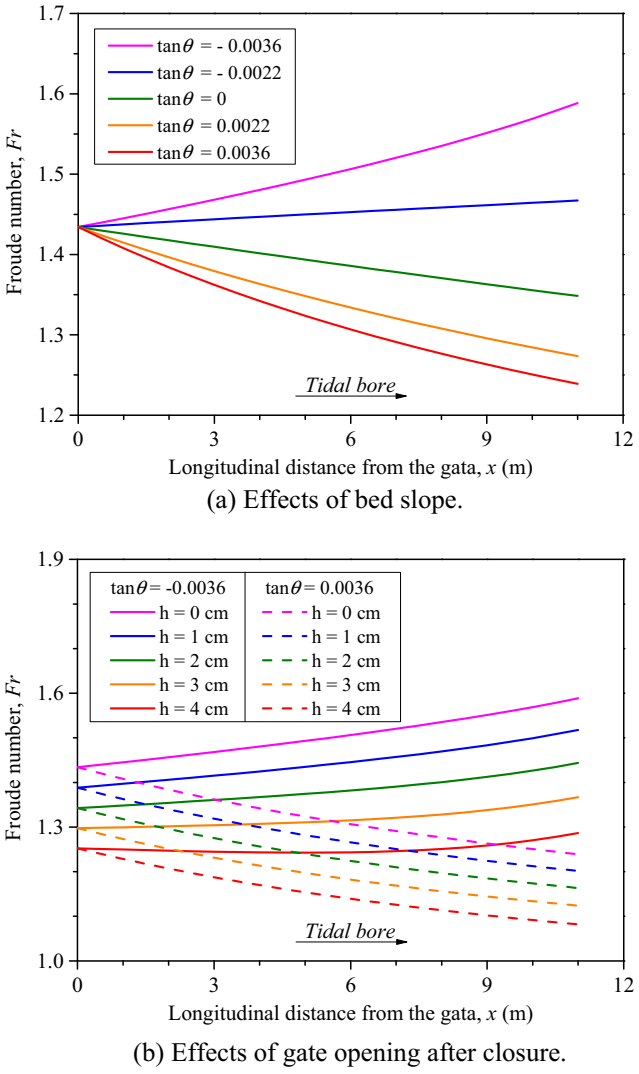

Fig. 5. Changes in Froude number as the tidal bore progresses up the slopes. (a) Effects of bed slope. (b) Effects of gate opening after closure.

little larger than the theoretical calculations. A main reason is that, in Eqs. (3) and (6), the free surface is assumed to be stationary, i.e., $\vec{V}.\vec{n} = 0$ at the free surface. However, it is not the case in practice. The differences increase with a decrease in slope. The absolute average errors were 1.5, 1.7, 1.75, 1.8 and 1.95 cm with channel slopes of 0.0036, 0.0022, 0, −0.0022 and −0.0036, respectively.

Fig. 5 illustrates the changes in Froude number as the tidal bore progresses up the channel slope, based upon the theoretical calculations. When the tidal bore progresses on a small slope with a positive slope angle, the bore Froude number decreases with increasing distance from the gate. Conversely, with a tidal bore progressing on a small negative slope, the Froude number increases along the channel (Fig. 5a). The Froude number decreases with the increase of the gate opening (after closure) as seen in Fig. 5b. More generally the Froude number characterises the bore free-surface profile. In the present experiments, for $Fr \leq 1.25$, an undular bore with smooth profile was observed; for $Fr \geq 1.5$, the breaking bore was characterised by a foaming/breaking front; for $1.25 < Fr < 1.5$, undular bores with some slight cross waves or breaking wave were observed. The latter pattern is sometimes described as a weak breaking bore with secondary waves [1].

6. Conclusion

Tidal bores progressing upstream on a small slope were analysed based upon both new physical data and theoretical calculations, with both positive and negative slope angles. The results indicate that the Froude number and the conjugate water depth ratio vary in response to changes in the bed slope. A general relationship is obtained for the conjugate depth ratio as a function of the Froude number and channel slope, and Eq. (14) gives a simplified expression. The conjugate depth ratio increases with an increasing Froude number and increases with a decrease in channel slope. The calculations show that the bore celerity and conjugate water depth results reproduced well the measured data for a relatively wide range of flow conditions in terms of bed slope, initial discharge and gate opening after closure.

Using the theoretical model, the changes in Froude number for a tidal bore progressing on the small slope channel with different slope angle and gate opening were calculated. The Froude number increases along the channel for a negative slope and decreases for a positive slope. The Froude number decreases with an increase in gate opening after closure at a particular channel slope.

Acknowledgments

This study was partially funded by the National Natural Science Foundation of China (Grant Nos. 51379190 and 50809062), China Scholarship Council and Zhejiang Association for International Exchange of Personnel. The authors acknowledge the technical assistance of Jason Van der Gevel and Matthews Stewart (The University of Queensland).

References

[1] X. Leng, H. Chanson, Turbulent advances of a breaking bore: preliminary physical experiments, Exp. Therm. Fluid Sci. 62 (2015) 70–77.
[2] H. Chanson, The Hydraulics of Open Channel Flow: An Introduction, Elsevier Butter-worth-Heinemann, Oxford, UK, 2004.
[3] P. Lubin, S. Glockner, H. Chanson, Numerical simulation of a weak breaking tidal bore, Mech. Res. Commun. 37 (2010) 119–121, http://dx.doi.org/10.1016/j.mechrescom.2009.09.008.
[4] A. Barré de Saint-Venant Théorie du Mouvement Non Permanent des Eaux, avec Application aux Crues des Rivières et à l'Introduction des Marées dans leur Lit Comptes Rendus des Séances de l'Académie des Sciences, Paris, France 73(4) (1871) 147–154.
[5] F.M. Henderson, Open Channel Flow, MacMillan Company, New York, USA, 1966.
[6] J.A. Liggett, Fluid Mechanics, McGraw-Hill, New York, USA, 1994.
[7] H. Chanson, Current knowledge in tidal bores and their environmental, ecological and cultural impacts, Environ. Fluid Mech. 11 (2011) 77–98, http://dx.doi.org/10.1007/s10652-009-9160-5.
[8] J. Chen, C. Liu, C. Zhang, H.J. Walker, Geomorphologic development and sedimentation in Qiantang Estuary and Hangzhou Bay, J. Coastal Res. 6 (1990) 559–572.
[9] P.A. Madsen, H.J. Simonsen, C.-H. Pan, Numerical simulation of tidal bores and hydraulic jumps, Coastal Eng. 52 (2005) 409–433.
[10] B.-Y. Lin, The Characteristics of the Qiantang River Tidal Bore, China Ocean Press, Beijing, 2008 (in Chinese).
[11] I. Ohtsu, Y. Yasuda, Hydraulic jump in sloping channels, J. Hydraul. Eng. 117 (1991) 905–921.
[12] D. Husain, A.A. Alhamid, A.-A.M. Negm, Length and depth of hydraulic jump in sloping channels, J. Hydraul. Res. 32 (1994) 899–910, http://dx.doi.org/10.1080/002216894094 98697.
[13] M. Beirami, M. Chamani, Hydraulic jumps in sloping channels: sequent depth ratio, J. Hydraul. Eng. 132 (2006) 1061–1068.
[14] H. Chanson, Turbulent shear stresses in hydraulic jumps and decelerating surges: an experimental study, Earth Surf. Process. Landforms 36 (2) (2011) 180–189, http://dx.doi.org/10.1002/esp.2031, 2 videos.

[15] J.B. Bélanger, Notes sur l'Hydraulique, Ecole Royale des Ponts et Chaussées, Paris, France, session 1841–1842, 223 pages, 1841.
[16] H. Chanson, Jean-Baptiste Bélanger, Hydraulic engineer and academic, engineering and computational mechanics, Proceedings of the Institution of Civil Engineers, UK 163(EM4) (2010) 227–233, http://dx.doi.org/10.1680/eacm.2010.163.4.227.
[17] C. Koch, H. Chanson, An Experimental Study of Tidal Bores and Positive Surges: Hydrodynamics and Turbulence of the Bore Front, Hydraulic Model Report No. CH56/05, Dept. of Civil Engineering, The University of Queensland, Brisbane, Australia, July, 170 pages, 2005.
[18] R. von Mises, Berechnung von ausfluss und uberfallzahlen, Z. ver. Deuts. Ing. 61 (1917) 447 (in German).
[19] H. Rouse, Advanced Mechanics of Fluids, John Wiley, New York, USA, 1959, 444 pages.